Self-narrowing of size distributions of nanostructures by nucleation antibunching

Frank Glas[1,*] and Vladimir G. Dubrovskii[2,3,4]

[1]*Centre for Nanoscience and Nanotechnology, CNRS, Université Paris-Sud, Université Paris-Saclay, Route de Nozay, 91460 Marcoussis, France*

[2]*St. Petersburg Academic University, Khlopina 8/3, 194021 St. Petersburg, Russia*

[3]*Ioffe Institute of the Russian Academy of Sciences, Politekhnicheskaya 26, 194021 St. Petersburg, Russia*

[4]*ITMO University, Kronverkskiy prospekt 49, 197101 St. Petersburg, Russia*

(Received 21 April 2017; published 31 August 2017)

We study theoretically the size distributions of ensembles of nanostructures fed from a nanosize mother phase or a nanocatalyst that contains a limited number of the growth species that form each nanostructure. In such systems, the nucleation probability decreases exponentially after each nucleation event, leading to the so-called nucleation antibunching. Specifically, this effect has been observed in individual nanowires grown in the vapor-liquid-solid mode and greatly affects their properties. By performing numerical simulations over large ensembles of nanostructures as well as developing two different analytical schemes (a discrete and a continuum approach), we show that nucleation antibunching completely suppresses fluctuation-induced broadening of the size distribution. As a result, the variance of the distribution saturates to a time-independent value instead of growing infinitely with time. The size distribution widths and shapes primarily depend on the two parameters describing the degree of antibunching and the nucleation delay required to initiate the growth. The resulting sub-Poissonian distributions are highly desirable for improving size homogeneity of nanowires. On a more general level, this unique self-narrowing effect is expected whenever the growth rate is regulated by a nanophase which is able to nucleate an island much faster than it is refilled from a surrounding macroscopic phase.

DOI: 10.1103/PhysRevMaterials.1.036003

I. INTRODUCTION

Size homogeneity within ensembles of nano-objects is highly desirable for improving the fundamental properties of nanomaterials as well as enhancing the characteristics of functional nanostructures and nanodevices. In particular, a high degree of size uniformity is paramount for photonic applications of semiconductor quantum dots [1], nanowires (NWs), and NW-based heterostructures [2]. Considerable effort has been made in the past to narrow the size distributions of nanostructures, using various means [3–20]. One well-known effect which degrades the size uniformity is associated with kinetic fluctuations and leads to the so-called Poissonian broadening of the size distributions [15,18]. In systems with time and size-independent instantaneous growth rates, the size distributions are Poissonian, with the variance scaling as the mean size and hence increasing infinitely with time [18]. Suppression of this broadening has previously been demonstrated, for example in the case of Stranski-Krastanow (Ge,Si) and (In,Ga)As quantum dots. A complex interplay between elastic stress relaxation, elastic interactions, time-dependent wetting layer thickness, surface energy constraints, and shape transformations may indeed result in a kinetic narrowing of their size distributions under appropriate growth conditions [5–14].

The recent development of semiconductor NWs grown by the vapor-liquid-solid (VLS) method (see Ref. [15] for a detailed review) has stimulated studies of their size distributions (for both diameters and lengths) and of possible ways to reduce widths of these distributions. In self-catalyzed III-V NWs, self-equilibration of the diameter distributions to a δ-like shape has been demonstrated theoretically [16–18] and confirmed experimentally for gallium-catalyzed GaAs NWs [16]. As regards the length distributions (LDs), kinetic narrowing effects have been observed either at a certain moment of time [19] (due to different growth rates of differently sized Ge NWs) or in ensembles of interacting GaN NWs [20] (due to interwire exchange of re-emitted growth species). However, fluctuation-induced broadening and nucleation randomness persist in the general case and lead to disappointingly broad NW LDs, in spite of many efforts.

On the other hand, VLS NWs present an interesting example of a system whose growth behavior and physical properties are determined by the supersaturation dynamics in nanosized catalysts [21–27]. Recent studies have revealed the following important features of the VLS growth of III-V NWs:

(i) During the growth of any given NW, there exists a temporal anticorrelation between the random individual nucleation events that mediate the formation of each monolayer (ML) from the catalyst nanodroplet. This is due to (1) the small size of this droplet, in which at least one NW constituent which strongly affects supersaturation is present at low concentration (here, the group-V species), and (2) the short time needed to complete a ML after nucleation, compared with the waiting time between nucleation events. Then, the droplet supersaturation plummets when a new ML forms, which leads to an exponential decrease of the probability for another nucleation to occur immediately after [21–27]. This effect has been termed "nucleation antibunching."

(ii) Nucleation antibunching leads to a saturation of the variance of the probability to form n MLs during a given time

*Corresponding author: frank.glas@c2n.upsaclay.fr

[21,25,26] in a given NW, while the variance should scale linearly with the mean length for a Poissonian process with a time-independent nucleation probability [21,27].

(iii) In ensembles of NWs, if nucleation antibunching does not operate (for instance when, once formed, MLs extend slowly), the diffusion-induced growth of each NW results in LDs that are much broader than in the Poissonian case [28].

(iv) A slow nucleation of the NWs (long incubation time required to form the first ML of each NW) also leads to a broadening of their LDs [29,30].

So far, the theoretical studies of nucleation antibunching have been restricted to individual NWs [21,25–27]. This is partly due to an easier comparison with experiments [21]: in an ensemble of NWs, beyond growth dynamics, there are many causes of growth rate variability that are difficult to control and even to assess: different NWs may have different radii, different droplet contact angles or be subjected to different growth fluxes due to different local environments. This points out that the nucleation statistics in individual NWs and the statistical properties of a NW ensemble are clearly not the same thing. In the first case, one can only study the time fluctuations of the instantaneous growth rate or of the NW lengths grown during successive time intervals whereas in the second case one can access ensemble properties, such as the distributions of lengths grown over a certain time. On the other hand, if the NWs do not interact with each other, the statistical properties of the ensemble should somehow be related to those of individual NWs. These questions are at the core of the present work.

The combination of nucleation antibunching and of the stochastic nature of the nucleation and growth process should affect the LDs, but this has not been studied so far. Here, we thus examine in detail the influence on the ensemble LDs of three major effects: (i) nucleation antibunching, (ii) random initial nucleation of the NWs, and (iii) fluctuation-induced Poissonian broadening [15,18,27,30–32]. In particular, we investigate how, in the presence of nucleation antibunching, the dispersion of the times at which the various NWs actually start growing affects the LDs. As a model system, we consider the self-catalyzed VLS growth of III–V NWs or the gold-catalyzed VLS growth under group-III-rich conditions. The elongation rate of such objects is entirely determined by the group-V content of the catalyst droplets [33–35]. More generally, our considerations apply to nano-objects growing from a nanosize mother phase or nanocatalyst in the so-called mononuclear regime [25–27] (a single nucleation event mediates the formation of a mesoscopic growth unit, such as a ML for NWs) provided (1) the nucleation event and the formation of the growth unit are much faster than the refill of the mother phase by the external fluxes, and (2) the nucleation rate depends exponentially on the number of atoms of a constituent that are dissolved in the mother phase.

Our main goal is to show that the supersaturation dynamics completely suppress the fluctuation-induced broadening of the LDs and impart to the NW ensemble a self-regulatory behavior with a variance which rapidly becomes time-independent. To this end, we perform, compare, and discuss several calculations of the LDs for ensembles of NWs. The system is described by the rate equations that are standard in nucleation theory [15,36]. However, the time- and size-dependent rate constants are exponential, as in Refs. [21,25,26]. As will be detailed in Sec. II, this results from the exponential dependence of the nucleation probability on the nucleation barrier [15] whereas supersaturation varies approximately linearly with composition [21,25]. This feature is central in determining the statistical properties of the ensemble.

The presentation is organized as follows. Section II introduces our model, which divides the history of each NW into two stages with different stochasticities: stage 1 extends from the establishment of the growth fluxes to the random formation of the first solid ML; stage 2 corresponds to proper NW growth, which is dominated by nucleation antibunching. The next four sections propose different calculations of the LDs. The first two sections take into account the discrete character of NW growth, which proceeds by addition of single MLs following individual nucleation events. In Sec. III, the calculations are entirely numerical: the growth of each NW of a large ensemble is simulated separately (according to the model rules) and from this we straightforwardly extract the time evolution of the LDs. In Sec. IV, we use analytical results previously established for single NWs with nucleation antibunching to obtain exact analytical formulas for the LDs and their statistical properties. In the following two sections, we develop an approach based on a continuum growth approximation which yields the large time asymptotic behavior of the system in a much simpler form. Section V first derives a closed form expression of the Green's function of the problem. In Sec. VI, we convolute this function with the distribution of starting times of the NWs to obtain a simple analytical expression of the LDs.

The discrete and continuum approaches give very similar results and demonstrate that, whenever the exponential terms are present, the short-time correlations suppress the fluctuation-induced effects.

II. MODEL

We assume that, at time $t = 0$, the assembly of identical droplets that will give rise to the NW ensemble is formed but that no NW has started growing. Constant external fluxes are then switched on. We split the history of each NW into two phases, namely a NW nucleation stage (stage 1) of variable duration, up to the formation of the first solid ML, followed by a NW growth stage (2). We are primarily interested in the case of "difficult" NW nucleation, i.e., the case where the average time before forming the first ML is long compared to the average waiting time between successive MLs at stage 2. There are many possible reasons for such a difference (substrate and NW materials may be different, as well as droplet contact angle, droplet feeding processes, etc.).

In this case, at stage 1, the group-V concentration in the droplets should quickly reach its maximum value $c_{\max}$, at which, in the absence of solid growth, the desorption from the droplet (which depends only on concentration and temperature) balances exactly the intake of group V, determined by the vapor flux. For most droplets, NW nucleation will take a much longer time. We can then write the probability per unit time for forming the first ML of any NW as $p_0 = \pi\, R_b^2 J(\Delta\mu_{\max})$, with R_b the droplet base radius (assumed to remain constant at stage 1 and to be the same for all NWs), J the nucleation rate, and $\Delta\mu_{\max}$ the difference of chemical potential between liquid and solid at $c_{\max}$. With such a time-independent p_0, the

fraction of droplets that have not given rise to a NW at time t is $f_0(t) = \exp(-p_0 t)$.

As regards stage 2, we assume, as in Refs. [21] and [25], that the number $N(t)$ of group-V minority atoms in the droplet is significantly affected by each nucleation event and that its variations affect significantly the nucleation probability (NP) of a new ML, to be distinguished from the NW nucleation probability pertaining to stage 1. The NP is now $p = \pi R^2 J(\Delta\mu)$, where R is the NW radius and nucleation rate J is possibly defined by parameters different from those of stage 1. Most importantly, $\Delta\mu$ varies with time due to the variations of N. Namely, in terms of number of equivalent MLs in the droplet, $n = N/\delta$ (with δ the number of group-V atoms in a ML), n decreases instantaneously by a unit after each nucleation, whereas the droplet refilling is assumed to proceed at a constant rate v (which must equal the stationary average growth rate attained in the later stage of growth).

The Zeldovich nucleation rate depends exponentially on the nucleation barrier [15,21] and hence, in a range of group-V concentration where it is legitimate to linearize the variations of the chemical potential and to neglect desorption from the droplet, the Zeldovich NP can be written as in Ref. [21]:

$$p = \pi R^2 J(\Delta\bar{\mu}) \exp\left[\bar{c}\frac{\partial\Delta\mu}{\partial\bar{c}} i_*(\Delta\bar{\mu})\frac{(N-\bar{N})}{\bar{N}}\right]. \quad (1)$$

Here, the overlined quantities are the values in an arbitrary reference state of chemical potential $\Delta\bar{\mu}$ (measured in thermal units), group-V concentration $\bar{c}$ and number $\bar{N}$ of group-V atoms in the droplet, and i_* is the corresponding number of III-V pairs in the critical nucleus [the introduction of which allows one to rewrite Eq. (3) of Ref. [21] without specifying the shape of the nucleus]. The NP thus varies exponentially with the number n of equivalent MLs in the droplet (defined above):

$$p(N) = p(\bar{N})\ \exp[\varepsilon\,(n-\bar{n})], \quad (2)$$

with

$$\varepsilon = \bar{c}\frac{\partial\Delta\mu}{\partial\bar{c}} i_*(\Delta\bar{\mu})\frac{1}{\bar{n}}. \quad (3)$$

This exponential dependence is the cause of the strong antibunching effect [21,25]. Indeed, the ratio of the NPs immediately after and before nucleation (which decreases the number of equivalent MLs in the droplet by 1), a constant of our model, is equal to $\gamma = e^{-\varepsilon}$. The larger ε, the more sensitive the NP to the number of atoms in the droplet and hence the more sub-Poissonian the process, with the limits $\varepsilon = 0$ ($\gamma = 1$) and $\varepsilon = +\infty$ ($\gamma = 0$) corresponding respectively to the Poisson and deterministic cases [25].

Let us introduce Ω_L, the average elementary volume per atom in the liquid phase ($0.02\,\text{nm}^3$ for liquid gallium), Ω_S, the volume of a III-V pair in the solid phase ($0.0452\,\text{nm}^3$ for GaAs), h, the height of a ML (0.326 nm for GaAs NWs growing along a (111) axis), and $f(\beta) = \pi(1-\cos\beta)(2+\cos\beta)/[3\,(1+\cos\beta)\sin\beta]$, the geometrical function relating the volume V of a spherical cap to the cube of its base radius R through the contact angle of the droplet β. Then, $\delta = \pi R^2 h/\Omega_S$ and $\bar{c} = \Omega_L \delta\bar{n}/V$. The antibunching parameter can thus be written as

$$\varepsilon = \frac{\pi\Omega_L}{f(\beta)\Omega_s}\bar{c}\frac{\partial\Delta\mu}{\partial\bar{c}} i_*(\Delta\bar{\mu})\frac{h}{\bar{c}R}. \quad (4)$$

Although this antibunching parameter may take substantial values in very narrow NWs or for a catalyst with extremely low group-V solubility, it may remain much smaller than 1 even in truly nanosized wires; for example, it equals only 0.15 for a NW with $R = 50\,\text{nm}$ and $\beta = 135^\circ$ if we assume $\bar{c}(\partial\Delta\mu/\partial\bar{c}) = 1$, $\bar{c} = 0.03$, and $i_*(\Delta\bar{\mu}) = 9$. This justifies the use of the strong inequality $\varepsilon \ll 1$ in some of our analytical calculations (Secs. V and VI).

To summarize, the two main parameters of our model are ε, defining the degree of antibunching, and $\alpha = p_0/v$, measuring the NW nucleation delay at stage 1 relative to the upper layers, as in Ref. [30].

The calculations carried out in Secs. III and IV, which cover the entire history of the NWs, require the introduction of another parameter. According to our description of stage 1, the NP p_s at the beginning of stage 2 (just after forming the first ML) is the same for all NWs, although this first ML forms at different times t_s for each NW (the distribution of these times is simply given by $d\,f_0/dt$). In principle, the value of p_s could be calculated by considering the variations with concentration of the nucleation and desorption rates, but this would require introducing several other parameters. Moreover, the stage 2 dynamics can be fully computed by tracking the NP, rather than concentration [25]. We thus take p_s as an extra free parameter. Note however that p_s is likely to be larger than the stationary stage 2 NP v, since a difficult NW nucleation implies that $c_{\max}$ is larger than the stationary stage 2 concentration.

III. NUMERICAL SIMULATIONS

We first carry out numerical simulations over large ensembles of NWs (typically 2×10^5). We then show in Sec. IV that the results of these simulations may be reproduced perfectly via analytical calculations, based on our previous study dealing with single NWs [25].

The growth of each NW of the ensemble is simulated independently, as specified by our model (Sec. II). All NWs are geometrically uniform in that they have the same radius and droplet contact angle, but of course they acquire different lengths at a given time. The external fluxes are established at time $t = 0$. During stage 1, the probability per unit time of forming the first ML in a given NW is taken as constant (as discussed in Sec. II) and the instant when this occurs is drawn accordingly. This probability is written $p_0 = \alpha v$, with v the *stationary* growth rate at stage 2, i.e., the probability of forming a new ML (NP) that compensates exactly the external fluxes. However, at stage 2, the NP varies with time, according to the following rules. In the intervals between nucleation events, the NP increases exponentially with time according to Eqs. (1) and (2), simply because the number of group-V atoms in the droplet increases linearly due to refill by the external fluxes. When a nucleation occurs (which is determined randomly according to the increasing instantaneous NP), it is followed instantaneously by the formation of a full ML; according to the same equations, this instantaneously decreases the NP to a fraction $\gamma = e^{-\varepsilon}$ of its prenucleation value. As mentioned in

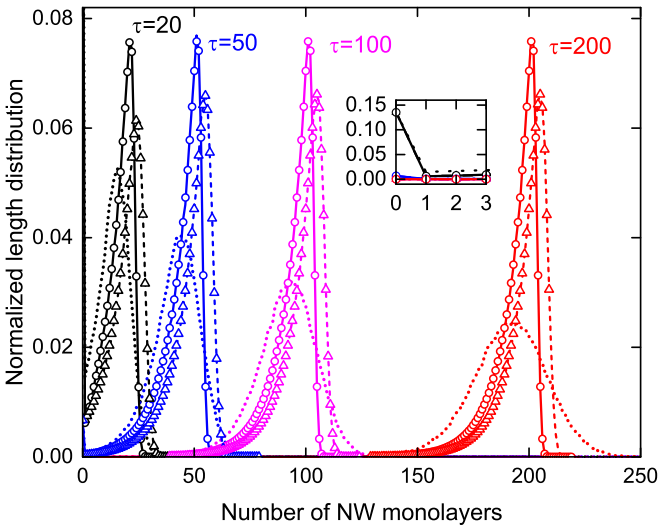

FIG. 1. Nanowire LDs after different growth times τ (given in units of the stationary waiting time ν^{-1} between MLs at stage 2) for the Poisson process ($\varepsilon = 0$, $\gamma = 1$, dots) and for weakly ($\varepsilon = 0.1$, $\gamma = 0.9048$, dashes) and moderately ($\varepsilon = 0.3$, $\gamma = 0.7408$, full lines) sub-Poissonian processes. Fixed parameters: $\alpha = 0.1$, $p_s = 2\nu$. The lines give the results of the numerical growth simulations (note that the function is only defined for integer values of the ML number) and symbols those of the analytical calculations of Sec. IV. Inset shows details of the distributions for small ML numbers.

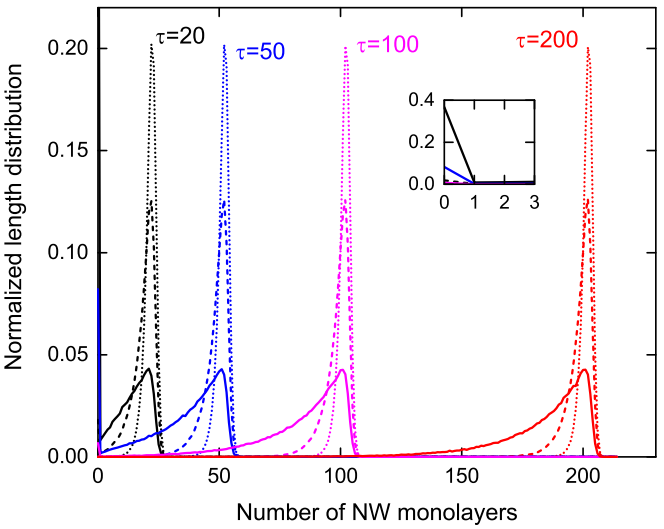

FIG. 2. Same as Fig. 1 for various values of the parameter α measuring the difficulty of forming the first NW ML from a droplet resting on the substrate: $\alpha = 0.5$ (dots), $\alpha = 0.2$ (dashes), $\alpha = 0.05$ (full lines). Fixed parameters: $\varepsilon = 0.3$, $p_s = 2\nu$. For sake of clarity, the analytical results are not shown.

Sec. II, we must also specify the NP p_s at the very beginning of stage 2 (i.e., the probability of forming a second ML). In each calculation, we assume that all NWs of the ensemble are characterized by the same parameters ε, α, ν, and p_s. For the first three parameters, this follows from assuming a uniform geometry for all NWs and droplets; for p_s, this follows from the quick attainment of fixed concentration $c_{\max}$ in nearly all droplets at stage 1.

Figures 1–3 show the evolution with time of the LDs for various degrees of nucleation antibuching at stage 2 (Fig. 1), increasingly difficult NW nucleation (Fig. 2), and various values of the NP at beginning of stage 2 (Fig. 3).

In all cases, even for modest degrees of nucleation antibunching, the LD quickly converges to a given shape with a finite standard deviation, after which the LD simply gets translated uniformly with time. Hence, the ensemble LDs behave very similarly to the LDs of segments grown during consecutive equal times in a single NW, that we measured and calculated previously [21,25]. In particular, the standard deviations of both types of LDs saturate quickly as the average segment length (single NW) or NW length (NW ensemble) increases, and the saturation value decreases as the process becomes more sub-Poissonian (Fig. 4). Only in the pure Poissonian case (dotted curves in Fig. 1 and curve labeled $\varepsilon = 0$ in Fig. 4) does the width of the distribution increase indefinitely with time.

However, and as expected, for fixed stage 2 conditions (given ε), the shape of the distribution depends critically on the conditions at stage 1: the more difficult the nucleation of the first ML (the smaller α), the broader the distribution of NW nucleation times and hence the broader the tail of the LD on the short length side (Fig. 2). On the other hand, the value of the NP p_s at the beginning of stage 2 has only a small effect: for lower NPs, the LD is simply retarded but its profile is hardly modified (Fig. 3).

The variations of the standard deviation of the LD with time (Fig. 4) synthetize these conclusions. Figure 4 also shows that the joint effect of delayed NW nucleation and nucleation antibunching at stage 2 may produce a nonmonotonic variation of the standard deviation.

IV. EXACT ANALYTICAL CALCULATIONS

Remarkably, the numerical results of Sec. III may be recovered analytically by using the results of our previous

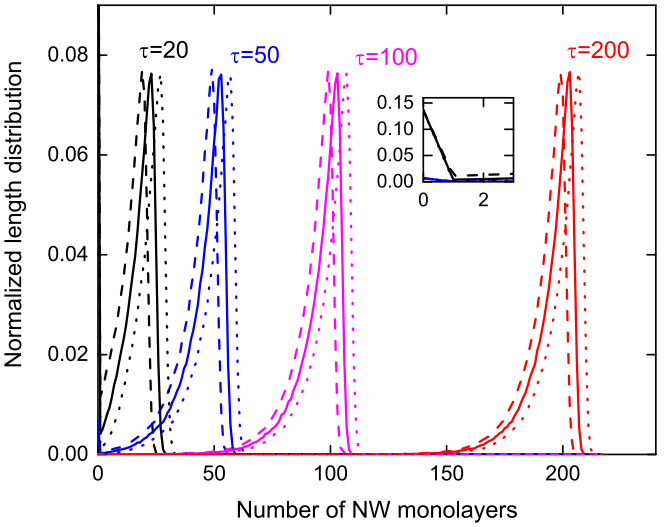

FIG. 3. Same as Figs. 1 and 2 for various values of the nucleation probability at the beginning of stage 2: $p_s = \nu$ (dashes), $p_s = 3\nu$ (full lines), $p_s = 10\nu$ (dots). Fixed parameters: $\varepsilon = 0.3$, $\alpha = 0.1$.

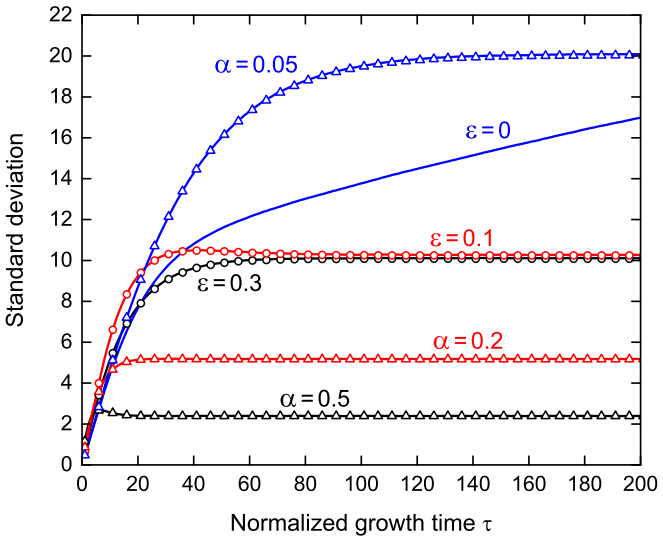

FIG. 4. Variation of the standard deviation of the length distribution with normalized growth time for various degrees of nucleation antibunching ε, at fixed $\alpha = 0.1$ and $p_s = 2v$ (curves labeled with ε values) and for decreasing NW nucleation probability α, at fixed $\varepsilon = 0.3$ and $p_s = 2v$ (curves labeled with α values). Lines: numerical growth simulations; symbols: analytical calculations of Sec. IV.

study devoted to single NWs [25]. There, we calculated the density of probability $\pi(t|p_s)$ for a second nucleation to occur after time t, conditional to the fact that a first nucleation occurred when the NP was equal to p_s (for given average growth rate v and antibunching degree γ or ε). From this quantity, we derived analytically the probability $\pi_n(T|p_s)$ that exactly n nucleations occur during a time interval of length T, conditional to the fact that the NP was p_s at the beginning of this interval, namely

$$\pi_n(T|p_s) = \sum_{m=0}^{n} \frac{g_{n-m}}{(\gamma;\gamma)_m} \exp[-\gamma^m E(T) p_s/(\varepsilon v)] \,, \tag{5}$$

where $(\gamma;\gamma)_m = (1-\gamma)(1-\gamma^2)\dots(1-\gamma^m)$ is a q-Pochhammer symbol [for $m \geqslant 1$, with $(\gamma;\gamma)_0 = 1$], $g_m = (-1)^m \gamma^{m(m-1)/2}/(\gamma;\gamma)_m$ and $E(T) = e^{\varepsilon v T} - 1$.

The conditional probability $\pi_n(\tau|p_s)$ is a powerful tool for calculating the time evolution of our ensembles of NWs. Indeed, the ensemble LD is simply given by the convolution of this probability with the distribution of times of formation of the first ML. Hence, the fraction of NWs which are n-ML long at time T (i.e., the LD) is

$$f_n(T) = \int_0^T p_0\, e^{-p_0 t}\, \pi_{n-1}(T-t|p_s)\, dt \quad \text{for } n \geqslant 1, \tag{6}$$

$$f_0(T) = e^{-p_0 T}. \tag{7}$$

Note that here we count the first ML, if any; for instance, 1-ML long NWs have acquired a first ML at the end of phase 1 and none in phase 2.

The LD can be expressed in terms of the incomplete gamma function $\gamma(s,x)$ (not to be confused with antibunching parameter γ) as

$$f_n(\tau) = \theta \rho^{-\theta} \sum_{m=0}^{n-1} \frac{g_{n-1-m}}{(\gamma;\gamma)_m} \exp[\alpha(m-\tau) + \rho e^{-m\varepsilon}] \times [\gamma(\theta, \rho e^{\varepsilon(\tau-m)}) - \gamma(\theta, \rho e^{-\varepsilon m})] \tag{8}$$

for $n \geqslant 1$, with $\theta = \varepsilon^{-1}\alpha = \varepsilon^{-1} p_0/v$, $\rho = \varepsilon^{-1} p_s/v$, and $\tau = vT$ the normalized growth time.

These formulas are exact for any values of parameters $\varepsilon \neq 0$, α, p_s and time τ and are computationally efficient unless ε is very small. The LDs so calculated agree extremely well with those obtained from our numerical simulations, as illustrated in Figs. 1 and 4 (hollow symbols). This confirms that for our identical and noninteracting NWs, the statistics of the ensemble may be calculated from those of the single NW.

The average length (in MLs) of the NW ensemble at time T is

$$\langle n(T)\rangle = \sum_{n=0}^{\infty} n\pi_n(T) = \int_0^T p_0 e^{-p_0 t} \sum_{n=1}^{\infty} n\pi_{n-1}(T-t|p_s) dt = 1 + e^{-p_0 T} + \int_0^T p_0 e^{-p_0 t} \sum_{n=0}^{\infty} n\pi_n(T-t|p_s) dt. \tag{9}$$

Using a generating function method as in Ref. [25] we find, after some calculations,

$$\langle n(\tau)\rangle = (\gamma;\gamma)_\infty \sum_{m=0}^{\infty} \frac{1}{(\gamma;\gamma)_m} \{1 - e^{-\alpha\tau} - \theta\rho^{-\theta} \exp[\alpha(m-\tau) + \rho e^{-m\varepsilon}][\gamma(\theta, \rho e^{\varepsilon(\tau-m)}) - \gamma(\theta, \rho e^{-\varepsilon m})]\} + 1 - e^{-\alpha\tau}. \tag{10}$$

Similarly, we can calculate the variance of the LD:

$$\sigma^2(\tau) = 2(\gamma;\gamma)_\infty \sum_{m=0}^{\infty} \frac{m - \mathcal{L}(\gamma)}{(\gamma;\gamma)_m} \{1 - e^{-\alpha\tau} - \theta\rho^{-\theta} \times \exp[\alpha(m-\tau) + \rho e^{-m\varepsilon}] [\gamma(\theta, \rho e^{\varepsilon(\tau-m)}) - \gamma(\theta, \rho e^{-\varepsilon m})]\} + 3\langle n(T)\rangle - \langle n(T)\rangle^2 - 2(1 - e^{-\alpha\tau}), \tag{11}$$

where $\mathcal{L}(\gamma) = \sum_{p=1}^{\infty} \gamma^p/(1-\gamma^p)$ is the Lambert series with unit coefficients.

V. GREEN'S FUNCTION OF CONTINUUM GROWTH EQUATION

The exact analytical solutions obtained in the previous section present the LDs as infinite series. We now develop a simplified approach based on a continuum growth equation of the Fokker-Planck type that will allow us to obtain much simpler analytic LDs for large enough NW lengths, and compare them to the exact results. The discrete set of the rate equations for the LDs can be written as [28,30]

$$\frac{df_n}{dt} = p_{n-1}(t) f_{n-1}(t) - p_n(t) f_n(t) \tag{12}$$

for all $n \geqslant 1$, with p_n the probability per unit time for a n-ML-long NW to form a new ML. Equation (12) means simply that the fraction of NWs having length n MLs at time t, $f_n(t)$, increases when one ML is added to NWs with length $n-1$ and decreases when one ML is added to NWs having this length n. Without group-V desorption, considering material balance for large enough number of NW MLs n yields

$$\bar{N} + \chi I \pi R^2 t = \frac{\pi R^2 h}{\Omega_S} n + N. \tag{13}$$

The left-hand side is the sum of the initial number of the group-V atoms dissolved in the droplet (which is taken identical to their reference number during growth for studying the Green's function) and the number of the group-V atoms arrived at the droplet from the vapor flux I by time t, with χ a geometrical coefficient [37].

Using Eq. (13) in Eq. (2), noting that the deposition rate is $v = \chi\, I\, \Omega_S / h$, and choosing the reference state such that $\pi R^2 J(\Delta\bar{\mu}) = v$, the NP can be put as

$$p_n(t) = p(vt - n) = v e^{\varepsilon(vt-n)}. \tag{14}$$

In terms of the dimensionless time, $\tau = vt$, Eq. (12) can be simplified to

$$e^{-\varepsilon\tau}\frac{df_n}{d\tau} = e^{-\varepsilon(n-1)} f_{n-1} - e^{-\varepsilon n} f_n = -\frac{\partial}{\partial n}(e^{-\varepsilon n} f_n) + \frac{1}{2}\frac{\partial^2}{\partial n^2}(e^{-\varepsilon n} f_n) - \ldots, \tag{15}$$

where we will keep only the two leading terms in the Taylor expansion (at the right-hand side) for $n \gg 1$ when $\varepsilon \ll 1$. In this case, the discrete rate equations are reduced to one Fokker-Planck equation:

$$e^{-\varepsilon\tau}\frac{\partial f(n,\tau)}{\partial \tau} = -\frac{\partial}{\partial n}[e^{-\varepsilon n} f(n,\tau)] + \frac{1}{2}\frac{\partial^2}{\partial n^2}[e^{-\varepsilon n} f(n,\tau)]. \tag{16}$$

Here, very unusually, the kinetic rate constant decreases exponentially with size n, due to nucleation antibunching, while it increases as a power of n in standard mean-field growth theories [31].

We now use the asymptotic method of Refs. [31,32] to find the Green's function of Eq. (16) corresponding to a δ-like initial condition. We introduce the modified variables

$$\rho = \frac{e^{\varepsilon n} - 1}{\varepsilon}; \quad z = \frac{e^{\varepsilon\tau} - 1}{\varepsilon} \tag{17}$$

and function $g(\rho, z)$ defined by

$$e^{-\varepsilon n} f(n,\tau) = g(\rho, z). \tag{18}$$

In these variables and at $\varepsilon \ll 1$, the Fokker-Planck equation takes the form

$$\frac{\partial g(\rho,z)}{\partial z} = -\frac{\partial g(\rho,z)}{\partial \rho} + \frac{1}{2}(1+\varepsilon\rho)\frac{\partial^2 g(\rho,z)}{\partial \rho^2}. \tag{19}$$

In Ref. [32], we showed that the ρ-dependent factor of the second derivative term of this equation can be changed to its mean value at $\rho = z$ with a high accuracy for narrow enough distributions (i.e., whose width is much smaller than the mean size z). In our case, this property is satisfied for $\varepsilon \ll 1$. Then, Eq. (19) has the asymptotic Gaussian solution for Green's function

$$G(\rho, z) = \frac{1}{\sqrt{2\pi}\sigma} \exp\left[-\frac{(\rho - z)^2}{2\sigma^2}\right], \tag{20}$$

where the z-dependent variance is given by

$$\sigma^2 = z + \frac{\varepsilon z^2}{2}. \tag{21}$$

This solution gives the δ-like LD at time $t = 0$, where $\sigma = 0$. Therefore, the Green's function determines the LD in the idealized case with all NWs nucleating at the same time. Using $\exp(\varepsilon n) = 1 + \varepsilon\rho$ in Eq. (18), the Green's function of Eq. (16) is thus obtained in the form

$$F(\rho, z) = \frac{1+\varepsilon\rho}{\sqrt{2\pi}\sigma} \exp\left[-\frac{(\rho - z)^2}{2\sigma^2}\right], \tag{22}$$

where the exponential dependencies of ρ and z on n and τ are specified by Eq. (17).

This solution is quite interesting since it combines the Poissonian and sub-Poissonian LDs. Indeed, at $\varepsilon = 0$ we simply have $\rho = n$ and $z = \tau$, which yields the Poissonian Green's function

$$F(n, \tau) = \frac{1}{\sqrt{2\pi\tau}} \exp\left[-\frac{(n - \tau)^2}{2\tau}\right] \tag{23}$$

with mean length $\langle n \rangle = \tau$ and variance $\sigma^2 = \tau$.

On the other hand, whenever $\varepsilon > 0$, the leading asymptotic term of the variance in Eq. (21) for large enough z is $\sigma^2(z) = \varepsilon z^2/2$ and the Green's function becomes a function of $\rho/z = \exp[\varepsilon(n-\tau)]$:

$$F(n - \tau) = \sqrt{\frac{\varepsilon}{\pi}} e^{\varepsilon(n-\tau)} \exp\left[-\frac{1}{\varepsilon}(e^{\varepsilon(n-\tau)} - 1)^2\right]. \tag{24}$$

The width of this LD is determined by the condition $|\exp[\varepsilon(n-\tau)] - 1| \cong \sqrt{\varepsilon}$ (defining where the Gaussian exponential is divided by factor e). The value of $\sqrt{\varepsilon}$ remains much smaller than unity for small enough ε. If we then use the linear approximation $\exp[\varepsilon(n-\tau)] - 1 \cong \varepsilon(n-\tau)$ in the exponential of Eq. (24), the $|n - \tau|$ values of interest are less than $1/\sqrt{\varepsilon}$. The $\exp[\varepsilon(n-\tau)]$ term is less than $\exp(\sqrt{\varepsilon}) \cong 1$. Therefore, for small ε and large n, the Green's function given by Eq. (16) is well approximated by the following Gaussian:

$$F(n - \tau) = \sqrt{\frac{\varepsilon}{\pi}} \exp[-\varepsilon(n-\tau)^2]. \tag{25}$$

Clearly, the mean length of this LD remains τ but the variance is time independent and equals $1/(2\varepsilon)$ rather than growing infinitely as in the Poissonian case. In other words, the Green's function depends on n and τ only via the combination $n - \tau$ and hence the shape of the LD is time invariant, as in Ref. [26]. Figure 5 shows how the asymptotic Green's functions given by Eq. (24) narrow up for larger ε, at a fixed time of 200.

VI. ANALYTIC LENGTH DISTRIBUTIONS IN THE CONTINUUM APPROACH

The Green's function obtained in Sec. V allows one to find the time evolution of the LDs for a given nucleation rate of

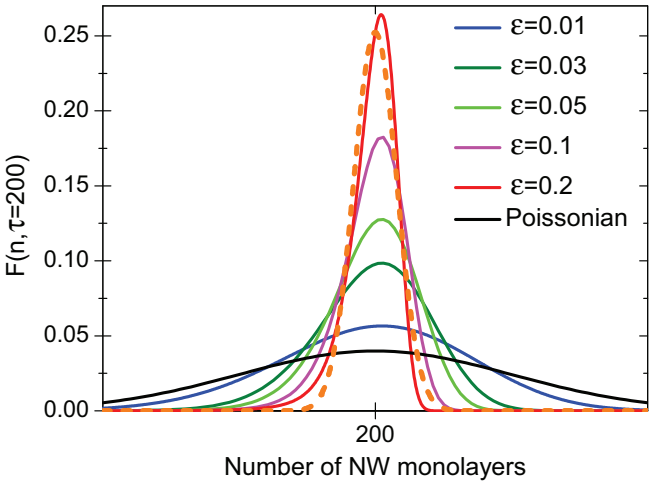

FIG. 5. Narrowing of Green's functions at a fixed τ of 200 with increasing values of ε, compared to the Poissonian LD. The dashed line shows the Gaussian approximation given by Eq. (25), for $\varepsilon = 0.2$.

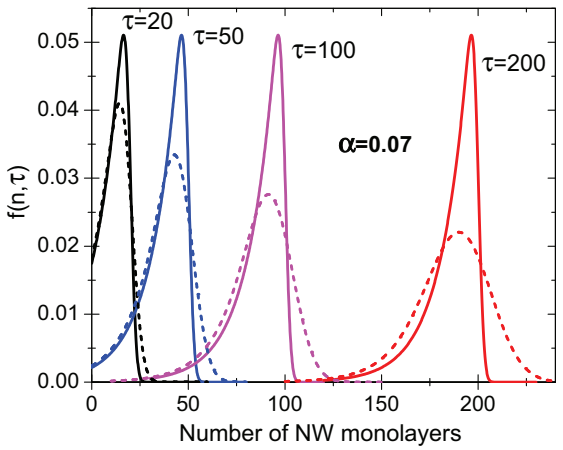

FIG. 6. Comparison between the time evolution of the NW LDs with nucleation-induced broadening in the presence (solid lines, $\varepsilon = 0.1$) and absence (dotted lines, $\varepsilon = 0$) of nucleation antibunching, for the same $\alpha = 0.07$.

NWs at $n = 0$ (end of stage 1). The latter is simply the product of the normalized density of droplets which have not yet given rise to a NW, $f_0(t)$, by the NP $p_0(t)$ of the very first NW ML, which in general depends on time. In a closed system where all droplets are formed initially (before exposure to the growth fluxes), f_0 obeys the equation

$$\frac{df_0}{dt} = -p_0(t) f_0(t). \tag{26}$$

If there is no significant NW nucleation delay, as considered in Ref. [28], the LDs should be well described by the Green's function itself. In the opposite case, where the NW nucleation stage takes a long time [29,38], we can use a time-independent p_0, as argued in Sec. II and assumed in Secs. III and IV. As already mentioned, we then have $f_0(t) = \exp(-p_0 t)$. In terms of the normalized time $\tau = vt$, the NW nucleation rate becomes

$$j(\tau) = \alpha\, e^{-\alpha\tau}, \tag{27}$$

with $\alpha = p_0/v$.

We reiterate that here the value of α should be smaller or even much smaller than unity, which means that nucleation of the very first NW ML from a droplet resting on the substrate surface is difficult compared to the upper layers. This feature leads to a pronounced asymmetry of the LDs toward a longer left tail representing shorter NWs, as indeed observed in experiments [29,30].

For any time-dependent NW nucleation rate, the NW LD $f(n,\tau)$ should be obtained by convolution of the Green's function with this nucleation rate [30,36], similarly to the discrete case studied in Secs. III and IV:

$$f(n,\tau) = \int_0^\infty dx\, F(n,\tau - x) j(x). \tag{28}$$

It is easy to convolute the asymptotic Gaussian Green's function given by Eq. (25) with the exponentially decreasing nucleation rate given by Eq. (27). The resulting asymptotic LD is the two-parametric function

$$f(n-\tau) = \frac{\alpha}{2} e^{\alpha(n-\tau)+\alpha^2/(4\varepsilon)} \mathrm{erfc}\left[\sqrt{\varepsilon}(n-\tau) + \frac{\alpha}{2\sqrt{\varepsilon}}\right]. \tag{29}$$

Here,

$$\mathrm{erfc}\,(y) = \frac{2}{\sqrt{\pi}} \int_y^\infty dt e^{-t^2} \tag{30}$$

is the complementary error function. This LD depends only on the difference $n - \tau$ and hence has a time-independent variance.

Without nucleation antibunching (at $\varepsilon \to 0$), convolution of the Poissonian Green's function given by Eq. (23) with the same exponential NW nucleation rate yields the result of Ref. [30], namely

$$f(n,\tau) = \frac{\alpha}{2} e^{\alpha(n-\tau)+\alpha^2\tau/2} \mathrm{erfc}\left[\frac{n - \tau + \alpha\tau}{\sqrt{2\tau}}\right]. \tag{31}$$

This LD can be obtained simply by changing the time-independent variance $1/(2\varepsilon)$ in the LD with antibunching to its Poissonian value τ, i.e., by setting $\varepsilon = 1/(2\tau)$ in Eq. (29). The LD given by Eq. (31) is also two-parametric; however, it depends differently on the two variables n and τ, with the variance increasing infinitely with τ. This important difference is demonstrated in Fig. 6. Both LDs at $\alpha = 0.07$ are broadened by the nucleation delay. However, the LD with nucleation antibunching at $\varepsilon = 0.1$ quickly acquires a time-independent shape with a longer left tail (toward small lengths), while the LD at $\varepsilon = 0$ continues spreading with time and asymptotically tends to a symmetrical Poissonian shape with the variance τ.

We have thus obtained an analytic asymptotic LD which should work well in situations with moderate nucleation antibunching ($\varepsilon \ll 1$) and a significant delay of the NW nucleation ($\alpha \ll 1$). At $\alpha \to 1$, this LD converges to the Gaussian Green's function given by Eq. (25). According to Eq. (29), upon completion of the NW nucleation step, the LD

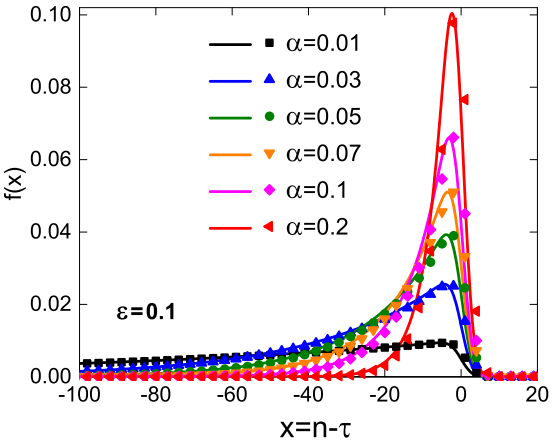

FIG. 7. Shapes of the universal LD at fixed $\varepsilon = 0.1$ and different α ranging from 0.01 to 0.2. Lines: continuum approximation [Eq. (32)]. Symbols: exact solution [Eq. (8)], for $p_s = v$; for sake of clarity, only one data point out of three is shown.

becomes a universal function of $x = n - \tau$,

$$f(x) = \frac{\alpha}{2} e^{\alpha x + \alpha^2/(4\varepsilon)} \mathrm{erfc}\left[\sqrt{\varepsilon} x + \frac{\alpha}{2\sqrt{\varepsilon}}\right]. \tag{32}$$

This distribution does not change shape in the subsequent growth stage and is translated uniformly with time. Suppression of kinetic fluctuations is due to nucleation antibunching in individual NWs. The universal LD depends on the two parameters, ε and α, describing the effects of antibunching and nucleation delay, respectively. Figure 7 shows how the universal LD at a fixed ε of 0.1 is broadened for smaller α, corresponding to longer NW nucleation delays. Figure 8 shows the narrowing of the LDs due to increasing the antibunching parameter ε, at a given $\alpha = 0.07$. This effect is stronger for smaller ε, while for larger ε the LDs converge to a shape that is simply determined by the duration of the NW nucleation step (stage 1).

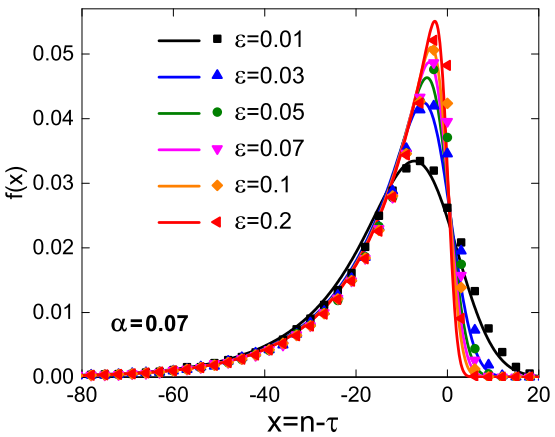

FIG. 8. Shapes of the universal LD at a fixed $\alpha = 0.07$ and different ε ranging from 0.01 to 0.2. Lines: continuum approximation [Eq. (32)] Symbols: exact solution for $p_s = v$, using Eq. (8) for $\varepsilon \geqslant 0.1$ and numerical simulation for $\varepsilon \leqslant 0.07$; for sake of clarity, only one data point out of three is shown.

For large enough τ, the function f defined in Eq. (32) has the following properties:

$$\int_{-\infty}^{\infty} dx\, f(x) = 1, \tag{33}$$

$$\int_{-\infty}^{\infty} dx\, x\, f(x) = -\frac{1}{\alpha}, \quad \int_{-\infty}^{\infty} dx\, x^2 f(x) = \frac{2}{\alpha^2} + \frac{1}{2\varepsilon}. \tag{34}$$

The first expression ensures the correct normalization of the asymptotic LDs to unity. Using Eqs. (33) and (34) and performing an integration by parts, we obtain the analytic mean size $\langle n \rangle$ and variance $\sigma^2 = \langle (n - \langle n \rangle)^2 \rangle = \langle n^2 \rangle - \langle n \rangle^2$ of this LD:

$$\langle n \rangle = \tau - \frac{1}{\alpha}, \quad \sigma^2 = \frac{1}{2\varepsilon} + \frac{1}{\alpha^2}. \tag{35}$$

Without nucleation antibunching, the mean size and variance are given by

$$\langle n \rangle = \tau - \frac{1}{\alpha}, \quad \sigma^2 = \tau + \frac{1}{\alpha^2}. \tag{36}$$

Therefore, as we saw earlier in the discrete calculations (Secs. III and IV) and for the Green's functions (Sec. V), the mean size is not influenced by antibunching whereas the variance is bounded with nucleation antibunching and grows infinitely without it. The variance given by Eq. (35) is the sum of two finite numbers, one describing the effect of antibunching and the other the nucleation delay. This explains the limited narrowing effect seen in Fig. 8 for large ε values, because the variance at $1/(2\varepsilon) \ll 1/\alpha^2$ nearly equals $1/\alpha^2$. In other words, nucleation antibunching completely suppresses the Poissonian fluctuation-induced broadening but does not correct the initial nucleation width of the NW LDs.

VII. COMPARISON OF THE TWO APPROACHES

Figure 9 shows a comparison between the LDs obtained from discrete Eq. (8) and continuum Eq. (29) and demonstrates

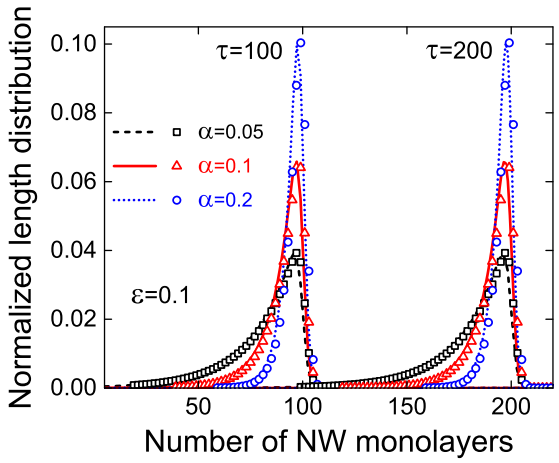

FIG. 9. Discrete (symbols) and continuum (lines) LDs obtained from Eqs. (8) and (29), respectively, for two different growth times and three different values of α (0.05, 0.1, and 0.2), at fixed $\varepsilon = 0.1$ and for $p_s = v$ in Eq. (8). For sake of clarity, only one data point out of two is shown.

their excellent quantitative correlation. The LD shapes are almost identical; however, the continuum LDs are slightly shifted toward smaller lengths. This is explained by the fact that in the continuum approximation, the NWs are assumed to emerge with zero length while actually they nucleate with a minimum length of 1 ML. We note that our continuum theory treats only the nucleation rate at zero length and tall enough nanowires with lengths $n \gg 1$, neglecting a transition region (NWs of length one in our case) [15,30]. Because of that, continuum LDs are insensitive to the parameter p_s introduced in Sec. II. As seen in Fig. 3, different p_s values do not change much the LD profiles but affect their expectations, i.e., the positions of the LD peaks. Recall that good fits are also obtained for the universal LD shapes, as shown in Figs. 7 and 8.

The variances of the LDs obtained numerically as the long time asymptotics to the exact Eq. (11) and from Eq. (35) are extremely close. We find that the former is independent of our parameter p_s and that, whatever the values of ε and α, the difference between the two is very close to $1/24$. This is strongly reminiscent of the corresponding factor $1/12$ found in Ref. [25] when studying analytically the LDs of very long consecutive segments grown for equal times in individual NWs [note also that the corresponding approximate variance, given by Eq. (56) of Ref. [25], is precisely double that given by Eq. (35) for infinite α], and we suspect that this could be demonstrated by using similar methods.

VIII. CONCLUSIONS

In conclusion, we have demonstrated by three different methods that nucleation antibunching in individual NWs, described by the antibunching parameter ε, completely suppresses the Poissonian broadening of LDs within ensembles of NWs. The initial nucleation randomness, described by the parameter α, affects the LDs forever, which is why the asymptotic variances and the LD shapes depend on the two parameters ε and α. However small these parameters may be, the LDs finally acquire time-independent shapes rather than spread infinitely with growth time. Numerical simulations over large ensembles of NWs and two different analytical approaches based on discrete and continuum rate equations yield very similar results. Recent experimental results confirm qualitatively our predictions by showing sub-Poissonian LDs of Ga-catalyzed GaAs NWs with a mean length of 4300 nm [39]. However, quantitative comparison with these data requires some care. In our analysis, we used a time-independent antibunching parameter throughout the entire growth process, while the GaAs NWs of Ref. [39] grow also in diameter, which affects the ε value. In addition, we assumed a time-independent NP for forming the first NW ML. This corresponds to the VLS regimes with long incubation times for NW growth (small α). Intermediate growth modes require further studies.

In our presentation, we used the language of VLS NWs growing in the mononuclear regime. We believe, however, that our results may have a broader range of application in systems whose NPs are given by the Zeldovich nucleation rate with a depletion effect that determines the degree of antibunching [40–42]. This central feature requires (i) a nanosized catalyst or other individual "growth regulator" and (ii) mononuclear growth. Overall, the sub-Poissonian size distributions presented here open up an interesting pathway for improving size homogeneity within ensembles of nanostructures.

ACKNOWLEDGMENTS

V.G.D. gratefully acknowledges financial support received from the Ministry of Education and Science of the Russian Federation under Grant No. 14.587.21.0040 (project ID RFMEFI58717X0040). This work was partially carried out within the framework of the CNRS-RFBR International Associated Laboratory ILNACS.

[1] S. Fafard, K. Hinzer, S. Raymond, M. Dion, J. McCaffrey, Y. Feng, and S. Charbonneau, Science **274**, 1350 (1996).
[2] O. L. Muskens, S. L. Diedenhofen, B. C. Kaas, R. E. Algra, E. P. A. M. Bakkers, J. G. Rivas, and A. Lagendijk, Nano Lett. **9**, 930 (2009).
[3] J. Tersoff, C. Teichert, and M. G. Lagally, Phys. Rev. Lett. **76**, 1675 (1996).
[4] J. A. Floro, E. Chason, R. D. Twesten, R. Q. Hwang, and L. B. Freund, Phys. Rev. Lett. **79**, 3946 (1997).
[5] F. M. Ross, J. Tersoff, and R. M. Tromp, Phys. Rev. Lett. **80**, 984 (1998).
[6] G. Medeiros-Ribeiro, A. M. Bratkovski, T. I. Kamins, D. A. A. Ohlberg, and R. Stanley Williams, Science **279**, 353 (1998).
[7] C. Teichert, M. G. Lagally, L. J. Peticolas, J. C. Bean, and J. Tersoff, Phys. Rev. B **53**, 16334 (1996).
[8] C. Chiu, Appl. Phys. Lett. **75**, 3473 (1999).
[9] P. Liu, Y. W. Zhang, and C. Lu, Phys. Rev. B **67**, 165414 (2003).
[10] P. Liu, Y. W. Zhang, and C. Lu, Phys. Rev. B **68**, 195314 (2003).
[11] P. Liu, Y. W. Zhang, and C. Lu, Phys. Rev. B **68**, 035402 (2003).
[12] K. Bromann, C. Felix, H. Brune, W. Harbich, R. Monot, J. Buttet, and K. Kern, Science **274**, 956 (1996).
[13] X. Peng, J. Wickham, and A. P. Alivisatos, J. Am. Chem. Soc. **120**, 5343 (1998).
[14] C. Ratsch, J. DeVita, and P. Smereka. Phys. Rev. B **80**, 155309 (2009).
[15] V. G. Dubrovskii, *Nucleation Theory and Growth of Nanostructures* (Springer-Verlag, Berlin, Heidelberg, 2014).
[16] V. G. Dubrovskii, T. Xu, A. Díaz Álvarez, G. Larrieu, S. R. Plissard, P. Caroff, F. Glas, and B. Grandidier, Nano Lett. **15**, 5580 (2015).
[17] J. Tersoff, Nano Lett. **15**, 6609 (2015).
[18] V. G. Dubrovskii, Phys. Rev. B **93**, 174203 (2016).
[19] V. G. Dubrovskii, T. Xu, Y. Lambert, J.-P. Nys, B. Grandidier, D. Stievenard, W. Chen, and P. Pareige, Phys. Rev. Lett. **108**, 105501 (2012).
[20] K. K. Sabelfeld, V. M. Kaganer, F. Limbach, P. Dogan, O. Brandt, L. Geelhaar, and H. Riechert, Appl. Phys. Lett. **103**, 133105 (2013).

[21] F. Glas, J. C. Harmand, and G. Patriarche, Phys. Rev. Lett. **104**, 135501 (2010).
[22] S. H. Oh, M. F. Chisholm, Y. Kauffmann, W. D. Kaplan, W. Luo, M. Rühle, and C. Scheu, Science **330**, 489 (2010).
[23] A. D. Gamalski, C. Ducati, and S. Hofmann, J. Phys. Chem. C **115**, 4413 (2011).
[24] C.-Y. Wen, J. Tersoff, K. Hillerich, M. C. Reuter, J. H. Park, S. Kodambaka, E. A. Stach, and F. M. Ross, Phys. Rev. Lett. **107**, 025503 (2011).
[25] F. Glas, Phys. Rev. B **90**, 125406 (2014).
[26] N. V. Sibirev, Tech. Phys. Lett. **39**, 660 (2013).
[27] V. G. Dubrovskii, Phys. Rev. B **87**, 195426 (2013).
[28] V. G. Dubrovskii, Y. Berdnikov, J. Schmidtbauer, M. Borg, K. Storm, K. Deppert, and J. Johansson, Cryst. Growth Des. **16**, 2167 (2016).
[29] F. Matteini, V. G. Dubrovskii, D. Rüffer, G. Tütüncüoğlu, Y. Fontana, and A. Fontcuberta i Morral, Nanotechnology **26**, 105603 (2015).
[30] V. G. Dubrovskii, N. V. Sibirev, Y. Berdnikov, U. P. Gomes, D. Ercolani, V. Zannier, and L. Sorba, Nanotechnology **27**, 375602 (2016).
[31] V. G. Dubrovskii, J. Chem. Phys. **131**, 164514 (2009)
[32] V. G. Dubrovskii and M. V. Nazarenko, J. Chem. Phys. **132**, 114507 (2010).
[33] C. Colombo, D. Spirkoska, M. Frimmer, G. Abstreiter, and A. Fontcuberta i Morral, Phys. Rev. B **77**, 155326 (2008).
[34] G. Priante, S. Ambrosini, V. G. Dubrovskii, A. Franciosi, and S. Rubini, Cryst. Growth Des. **13**, 3976 (2013).
[35] F. Glas, M. R. Ramdani, G. Patriarche, and J.-C. Harmand, Phys. Rev. B **88**, 195304 (2013).
[36] V. G. Dubrovskii and N. V. Sibirev, Phys. Rev. B **89**, 054305 (2014).
[37] F. Glas, Phys. Status Solidi B **247**, 254 (2010); **252**, 1897 (2015).
[38] B. Kalache, P. Roca i Cabarrocas, and A. Fontcuberta i Morral, Jpn. J. Appl. Phys. **45**, L190 (2006).
[39] E. Koivusalo, T. Hakkarainen, and M. Guina, Nanoscale Res. Lett. **12**, 192 (2017).
[40] Y.-C. Chou, W.-W. Wu, S.-L. Cheng, B.-Y. Yoo, N. Myung, L. J. Chen, and K. N. Tu, Nano Lett. **8**, 2194 (2008).
[41] A. O. Kovalchuk, A. M. Gusak, and K. N. Tu, Nano Lett. **10**, 4799 (2010).
[42] W. Theis and R. M. Tromp, Phys. Rev. Lett. **76**, 2770 (1996).